JOURNAL OF MATERIALS SCIENCE 22 (1987) 3885–3892

Further investigations on martensites in Fe–0.5 wt % C and Fe–0.5 wt % C–24 wt % Ni melt spun ribbons

FAWZY H. SAMUEL
Central Metallurgical Research and Development Institute, El-Tabbin, Helwan, P.O. Box Iron & Steel, Cairo, Egypt

The types of martensites occurring in Fe–C and Fe–Ni–C melt spun ribbons in the as-solidified and after heat treatment conditions has been investigated using transmission electron microscopy. It has been found that melt spinning of Fe–0.5 wt % C induces a dislocated martensitic structure at room temperature even for grains as fine as 3 μm. The martensite laths are separated by thin layers of retained austenite. The martensite/austenite orientations are controlled by both the K–S and N–W relationships. Some of the martensite laths exhibit a twin relation. The dislocations within the laths are mainly screw. The counterpart alloy, Fe–0.5 wt % C–24 wt % Ni exhibits 100% austenite under similar conditions. Increasing the austenite grain size upon annealing enhances martensitic transformation. The present work is concentrated on the details of butterfly martensite obtained in these ribbons.

1. Introduction

Martensite in Fe–C alloys ($\leqslant 0.3\%$ C) is a lath type, containing a high dislocation density. Occasionally twins are also observed. The dislocation density within the martensite laths is so high that individual dislocations cannot be resolved by the transmission electron microscope (TEM) [1]. Using electrical resistivity measurements, Speich [2] estimated the dislocation density to be between 0.3 and 0.9 $\times 10^{12}$ cm^{-3}. Thomas and co-workers could observe small amounts of retained austenite in low alloy steels [3]. According to their studies, the austenite–martensite orientations are controlled by the K–S and N–W relationships. The deviation between the close-packed directions, $[\bar{1}\,0\,1]_f$ and $[1\,1\,1]_b$, is 0° in the K–S relationship and 5.6° in the N–W relationship, but in many cases angles ranging between 0 and 5.6° are frequently observed. (The suffices f and b used for the crystallographic indices throughout the paper mean f.c.c. and b.c.c., respectively.)

In Fe–Ni–C alloys, four different martensite morphologies form, depending upon the formation temperature and composition, and for alloys of a fixed carbon content, the martensite morphology changes from lath to butterfly to lenticular to thin plates as the formation temperature is decreased [4]. Butterfly martensite exhibits a $\{2\,2\,5\}_f$ habit, contains several kinds of defects other than $\{1\,1\,2\}_b$ transformation twins and some but not all plates show mid-ribs. Lenticular martensite exhibits a $\{2\,5\,9\}_f$ habit and is partially twinned with a mid-rib. Umemoto *et al.* [5] have found that the austenite–martensite orientation relationship is $(1\,1\,1)_f \parallel (0\,1\,1)_b$ and $[1\,0\,1]_f$ is 2° from $[1\,1\,1]_b$. In general, the complex features of the substructures of butterfly martensite and the characteristics of $\{1\,1\,2\}_b$ twins and $\{1\,0\,1\}_b$ planar defects have been found to be quite similar to those observed in non-paired $\{2\,2\,5\}_f$ plate martensite.

Inokuti and Cantor [6] have reported that small as-solidified austenite grain size during splat-quenching causes a substantial depression of the martensite transformation temperature. Because of this suppression of the austenite reaction, splat quenched Fe–Ni alloys with $\geqslant 20\%$ nickel have a retained austenite microstructure. I have discussed previously [7, 8] the effect of austenite grain size and percent of retained austenite as a function of annealing temperature and cooling media, on the hardness and tensile properties of the present Fe–Ni–C ribbons. Also, the morphology, substructure and amount of transformed ferrite and/or martensite as a result of austenite decomposition in these ribbons were described. The present work was undertaken to investigate mainly by means of (TEM), the types of martensites occurring in Fe–C and Fe–Ni–C melt spun ribbons in the as-solidified conditions and after annealing at 800° C followed by quenching at different temperatures such as 25°, −60° and −196° C. The austenite–martensite orientation relationships were also studied.

2. Experimental procedures

A high purity Fe–24 wt % Ni–0.5 wt % C alloy and a commercial Fe–0.5wt % C steel were used in the present study. Specimens of these alloys were melt-quenched by a conventional melt-spinning technique [7], using copper and steel wheels as substrate. The reason for using a steel wheel for the Fe–0.5 wt % C alloy is to induce martensitic structure in the as-solidified structure as discussed previously [8, 9].

For annealing purposes, the specimens were

0022–2461/87 $03.00 + .12

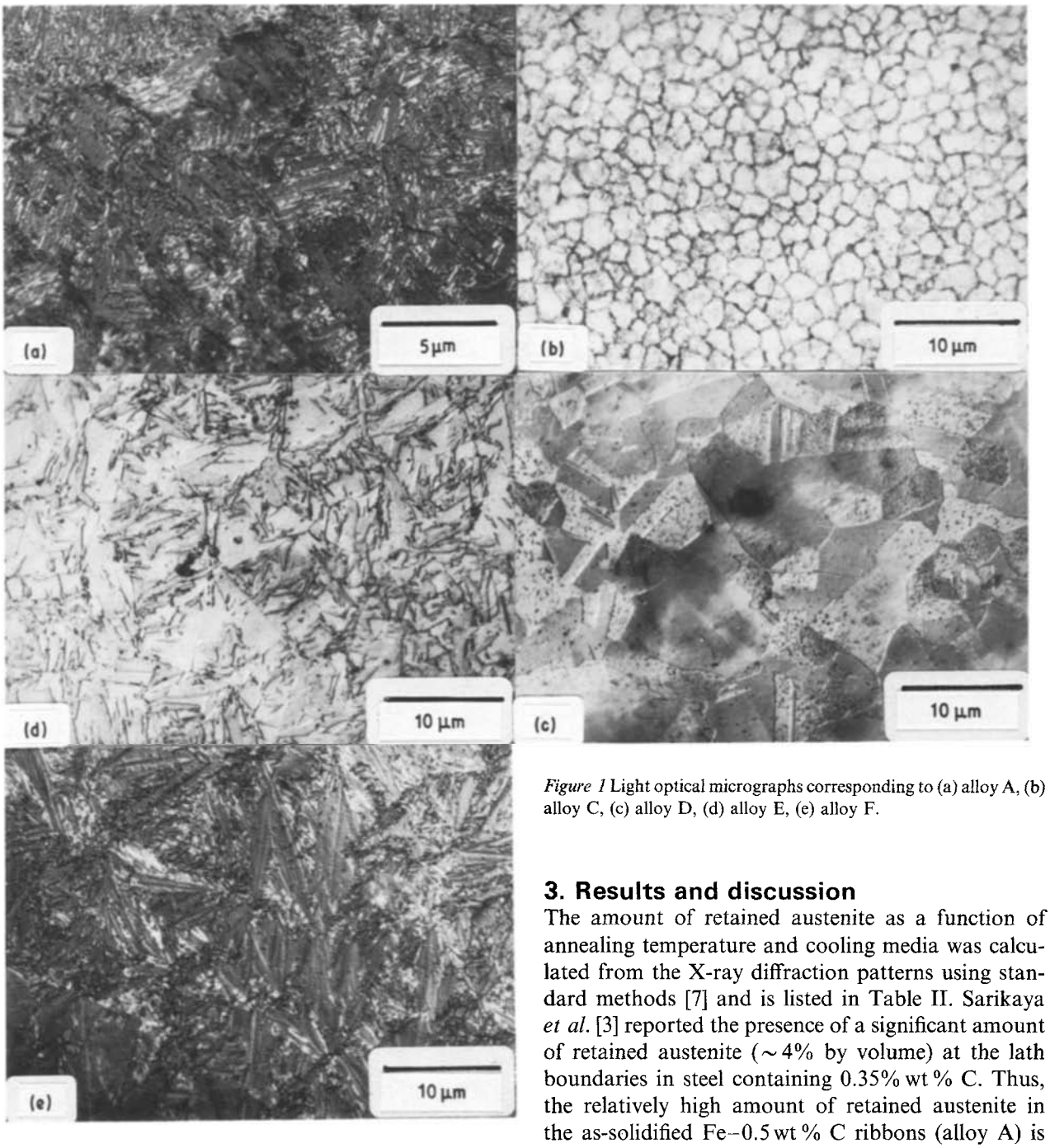

Figure 1 Light optical micrographs corresponding to (a) alloy A, (b) alloy C, (c) alloy D, (d) alloy E, (e) alloy F.

encapsulated in silica tubes (with addition of small amounts of pure niobium metal) and sealed under vacuum. The regime of heat treatment is given in Table I. X-ray diffractometry was carried out using CoKα radiation (λ = 0.1788 nm), on specimens pasted on glass plates using an amorphous glue. Specimens for optical microscopy, TEM, hardness as well as tensile tests were prepared using similar techniques mentioned elsewhere [7].

3. Results and discussion

The amount of retained austenite as a function of annealing temperature and cooling media was calculated from the X-ray diffraction patterns using standard methods [7] and is listed in Table II. Sarikaya *et al.* [3] reported the presence of a significant amount of retained austenite ($\sim$4% by volume) at the lath boundaries in steel containing 0.35% wt % C. Thus, the relatively high amount of retained austenite in the as-solidified Fe–0.5 wt % C ribbons (alloy A) is attributed to the relatively very fine grain size in alloy A ($\sim$2–3 μm) enhanced by rapid cooling (10^4–10^5 K s^{-1}). It should be noted that the M_s and M_f temperatures for Fe–0.5 wt % C alloy are, respectively, 250° and 100° C. Thus, cooling this alloy to −60° C would result in a great reduction in the amount of retained austenite to bring it to about 4%.

The M_s temperature of Fe–24 wt % Ni–0.5 wt % C is −35° C [10]. Increasing the grain size up to $\sim$12 μm followed by cooling to −60° C resulted in a

TABLE I Heat treatment regime

Alloy	Designation	Treatment
Fe–0.5 wt % C	A	As-melt quenched.
	B	A + cooled to −60° C, hold for 1 h.
Fe–24 wt % Ni–0.5 wt % C	C	As-melt quenched.
	D	C + annealed at 800° C for 1 h + ice brine quenched.
	E	C + annealed at 800° C for 1 h + cooled to −60° C, hold for 1 h.
	F	C + annealed at 800° C for 1 h + cooled to −196° C, hold for 1 h.

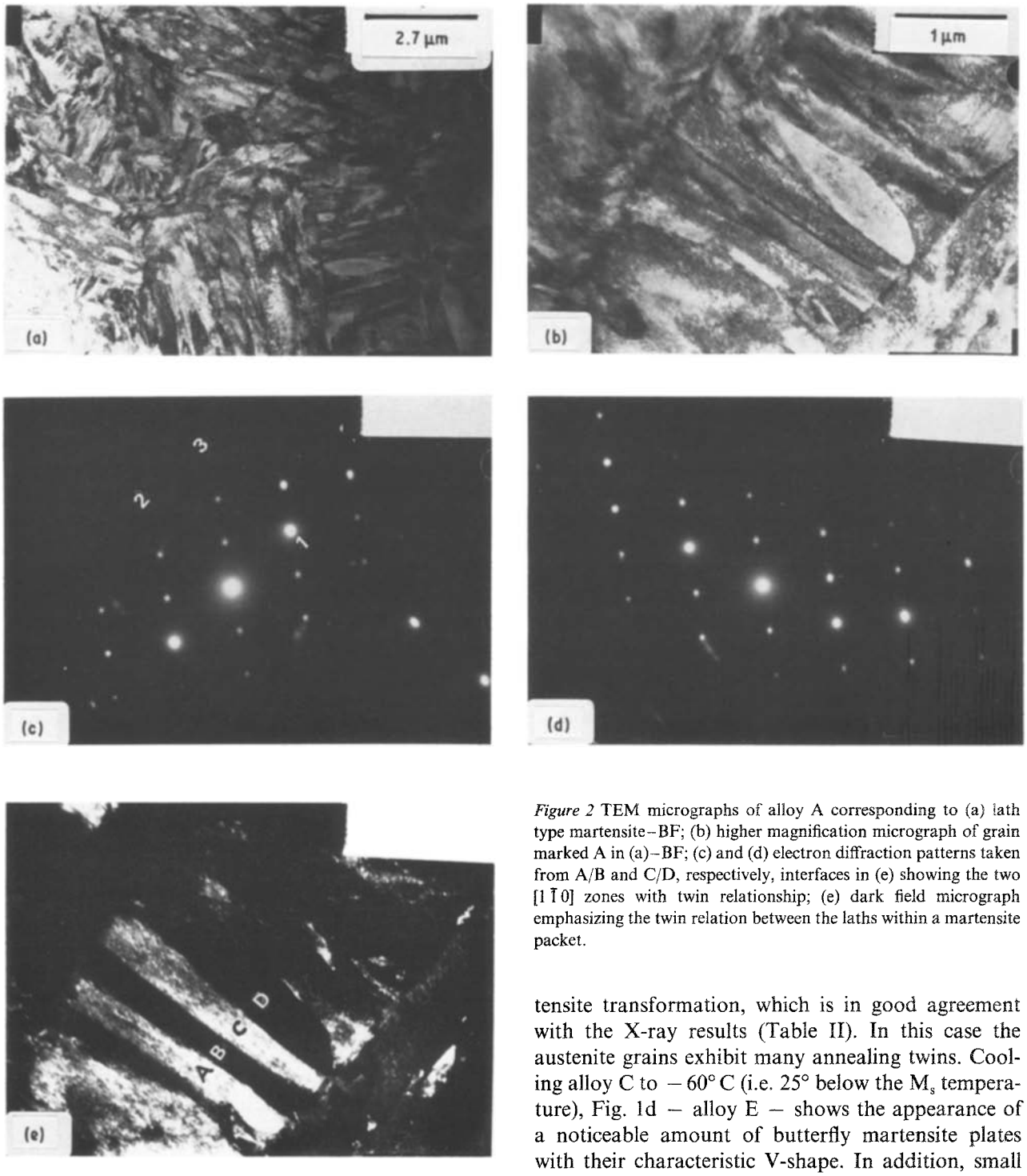

Figure 2 TEM micrographs of alloy A corresponding to (a) lath type martensite–BF; (b) higher magnification micrograph of grain marked A in (a)–BF; (c) and (d) electron diffraction patterns taken from A/B and C/D, respectively, interfaces in (e) showing the two [1 $\bar{1}$ 0] zones with twin relationship; (e) dark field micrograph emphasizing the twin relation between the laths within a martensite packet.

remarkable transformation of austenite into martensite. However, cooling to $-196°$ C did not approach the M_f temperature of this alloy. Our earlier measurements [11, 12] on the hardness of the solid state Fe–0.5 wt % C and Fe–24 wt % Ni–0.5 wt % C alloys cooled to the liquid nitrogen temperature are, respectively, 650 and 350 HV. The present high microhardness values are qualitatively as a consequence of Hall-Petch strengthening by the fine scale ferrite and martensite microstructures.

Fig. 1a is an optical micrograph of alloy A, showing complete martensite transformation having the form of packets. Many of these packets extend from one side of the grain boundary to the opposite side. In the case of alloy C, Fig. 1b reveals a complete austenite microstructure with grain size not more than 3 μm. For alloy D, Fig. 1c does not show evidence of martensite transformation, which is in good agreement with the X-ray results (Table II). In this case the austenite grains exhibit many annealing twins. Cooling alloy C to $-60°$ C (i.e. 25° below the M_s temperature), Fig. 1d – alloy E – shows the appearance of a noticeable amount of butterfly martensite plates with their characteristic V-shape. In addition, small amounts of burst type martensite are frequently observed. Decreasing the transformation temperature to $-196°$ C, alloy F, results in the formation of lenticular martensite plates having mid-ribs, Fig. 1e. Thus the sequence of martensite formation is in good accordance with transformation temperature and nickel content as mentioned in the introduction.

Fig. 2a shows a typical (TEM) of the martensite

TABLE II Some properties of the alloys studied

Alloy	% Retained Austenite	Grain Size (μm)	Hardness (HV)
A	14	4	750
B	4	4	800
C	100	3	325
D	100	12	300
E	73	12	430
F	35	12	540

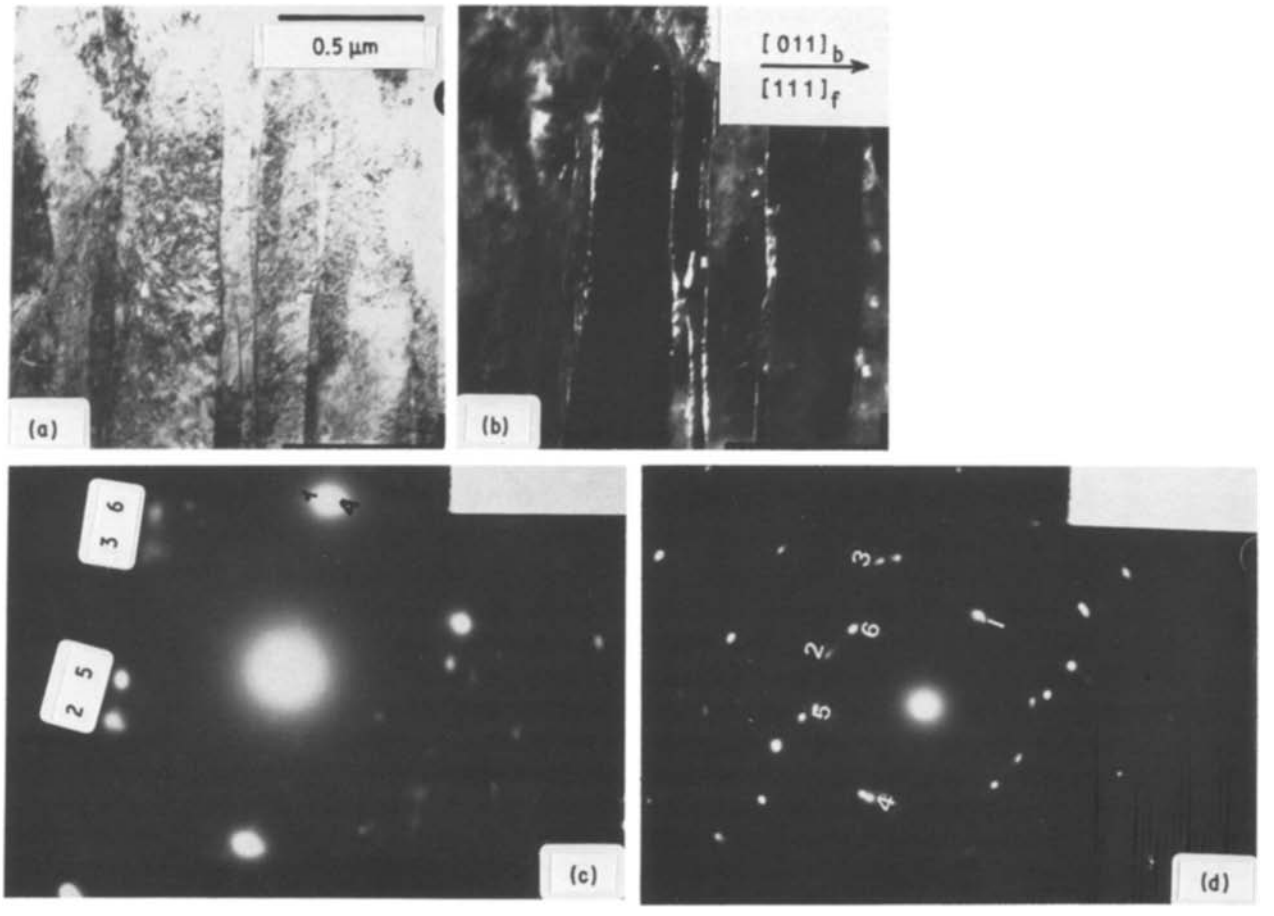

Figure 3 TEM micrographs corresponding to alloy B: (a) lath type martensite–BF; (b) retained austenite–DF; (c) an electron diffraction pattern showing $(1\,1\,1)_f \sim \| (0\,1\,1)_b$; (d) an electron diffraction pattern showing $(1\,1\,1)_f \sim \| (0\,1\,1)_b$.

microstructure in alloy A. Fig. 2b is a higher magnification micrograph of a packet in Fig. 2a. This packet contains several laths approximately parallel to each other. The average lath length is $\sim 2\,\mu m$ and the lath width is $\sim 0.3\,\mu m$. Selected area diffraction patterns, Figs. 2c and d, were obtained from adjacent laths A to D marked in Fig. 2e. Each diffraction pattern could be analysed as two super-imposed $[1\,\bar{1}\,0]$ zones which indicated an exact twin relationship between lath orientation. The dark field micrograph in Fig. 2e shows that the two orientations are observed with every alternate lath. Many packets of laths in alloy A contained twin-related laths, and the morphology of these packets was almost always similar to that shown in Fig. 2.

As shown in Table II, a considerable amount of retained austenite was detected in alloy B. The existence of this parent phase at $-60°$ C in this steel has been attributed to several stabilizing mechanisms, one being the high carbon content in austenite. A suggestion has been made [13] that a small grain size causes Hall-Petch strengthening of the austenite and therefore greater resistance to martensite transformation shear stresses. For determining the exact austenite–martensite orientation relationship, the diffraction patterns (for indexing of electron diffraction patterns see Table III) were taken in the orientation $(1\,1\,1)_f \| (0\,1\,1)_b$. There is no measurable deviation between the planes $(1\,1\,1)_f$ and $(0\,1\,1)_b$ in these diffraction patterns, although the two zones used deviated by about 60°. In Fig. 3a many adjacent laths, separated by retained austenite, can be seen. Fig. 3b exhibits a dark field image taken using the $(0\,2\,0)_f$ reflection. The diffraction patterns (for example see Fig. 3c) taken at the lath boundaries when the orientation of the specimens is $[1\,0\,1]_f$ and $[\bar{1}\,1\,1]_b$ showing parallelism between the planes $(1\,1\,1)_f$ and $(0\,1\,1)_b$, confirming the K–S relationship. It was found that each lath uniquely obeyed the same variant of the austenite–martensite orientation relationship. The deviation in the directions $[\bar{1}\,0\,1]_f$ and $[1\,1\,\bar{1}]_b$ is not always 0°. This fact can easily be seen from Fig. 3d, which is an electron diffraction pattern taken from a micrograph similar to that of Fig. 3a. As can be seen, the plane $(1\,1\,1)_f$ is 2° away from the $(0\,1\,1)_b$ plane whereas the zones $[1\,\bar{1}\,0]_f$ and $[1\,0\,0]_b$ appear to be parallel, which is expected from the relationship.

A typical example of internally twinned laths is displayed in Fig. 4a. The twins have the form of thin striations. Fig. 4b is an electron diffraction pattern

TABLE III Indexing of the electron diffraction patterns

Figure No.	Spot No./Plane			Nearest zone axis
2c	1/(1 1 0)	2/(1 1 2)	3/(0 0 2)	$[\bar{1}\,1\,0]_b$
3c	1/(0 1 1)	2/(1 0 $\bar{1}$)	3/(1 1 0)	$[\bar{1}\,\bar{1}\,1]_b$
	4/(1 1 1)	5/($\bar{1}$ 1 $\bar{1}$)	6/(0 2 0)	$[\bar{1}\,0\,1]$
3d	1/(0 1 1)	2/(0 $\bar{1}$ 1)	3/(0 0 2)	$[1\,0\,0]_b$
	4/($\bar{1}$ $\bar{1}$ $\bar{1}$)	5/($\bar{1}$ $\bar{1}$ 1)	6/(0 0 2)	$[\bar{1}\,1\,0]_f$
4b	1/(1 1 0)	2/($\bar{1}$ 2 1)	3/($\bar{2}$ 1 1)	$[1\,\bar{1}\,3]_b$
	4/(0 1 1)	5/(1 $\bar{1}$ 2)	6/(1 $\bar{2}$ 1)	$[3\,1\,\bar{1}]_T$
7	1/(1 1 1)	2/(3 $\bar{1}$ 1)	3/(2 $\bar{2}$ 0)	$[1\,1\,\bar{2}]_f$
	4/(0 1 1)	5/(2 1 1)	6/(2 0 0)	$[0\,1\,\bar{1}]_b$

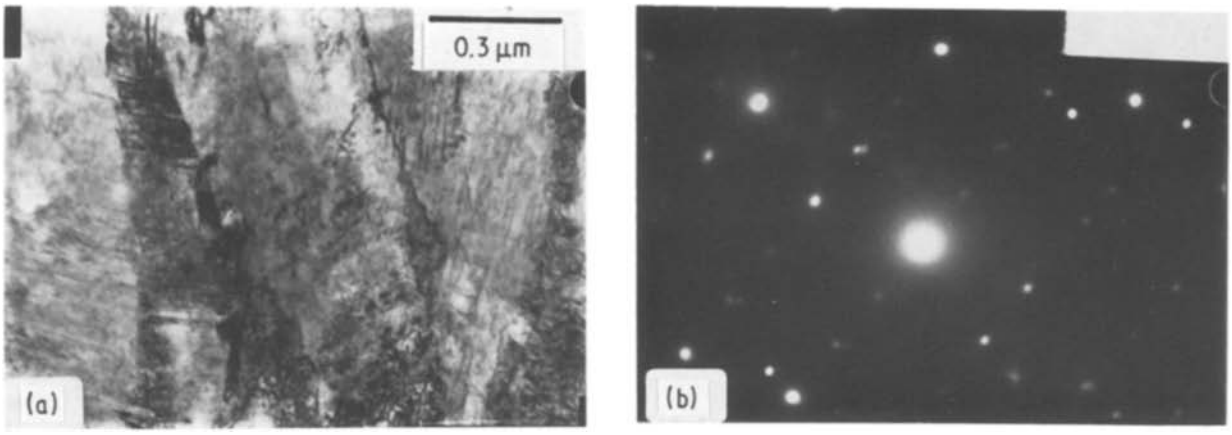

Figure 4 TEM micrographs corresponding to alloy B: (a) twinned laths – BF; (b) an electron diffraction pattern showing zone order $[1\,\bar{1}\,3]$ and $[3\,1\,\bar{1}]$ laue zones.

corresponding to the twinned laths and comprising two superimposed zero order $[1\,\bar{1}\,3]$ and $[3\,1\,\bar{1}]$ Laue zones centred on the electron beam. Trace analysis of the fine scale internal twins revealed that they were parallel to $\{1\,1\,2\}$ planes. Fig. 5a exhibits an isolated martensite lath oriented near $[1\,0\,0]_b$. This micrograph contains two sets of dislocations perpendicular to each other. Using various two beam conditions, both dislocations are visible for the reflection $(0\,0\,2)_b$, Fig. 5b, whereas one of them is invisible in the reflection $(0\,1\,1)_b$, Fig. 5c, indicating that these dislocations are in the screw orientation; the contrast images reveal that the Burgers vector of dislocations in the direction $[0\,\bar{1}\,1]_b$ is $a/2[1\,\bar{1}\,1]$ and the Burgers vector of dislocations in the direction $[0\,1\,1]$ is $a/2[\bar{1}\,1\,1]$.

Umemoto *et al.* [5] have studied the crystallographic and substructural features of butterfly martensite occurring in Fe–Ni–Cr–C alloy by means of TEM. Their results show two types of butterfly martensites marked as type A and type B. Type A is characterized by smooth and straight martensite/austenite interfaces, while type B is usually larger than type A and is characterized by thicker wings, somewhat curved martensite–austenite interfaces and the existence of a mid-rib. For both type A and type B, the angle between the wings is about 136°.

Fig. 6a exhibits the appearance of butterfly martensite plates at an austenite grain boundary in alloy E. Higher magnification micrographs reveal that the angle between the two plates forming a butterfly morphology is about 40 or 140°, for example see Fig. 6b. The transformation twins are observed covering the entire width of the plates and making the same angles i.e. 40 or 140° with respect to the martensite–austenite interface. Fig. 6c displays a butterfly martensite exhibiting $(0\,1\,1)_b$ planar defects. It is seen from this figure that one of the martensite–austenite interfaces is not smooth as in the case described in Fig. 6a and it is rather irregular. These irregularities are arising from the extension of the $[0\,1\,1]_b$ planar defects within the plate into the austenite slip on the $(1\,1\,1)_f$ plane. The

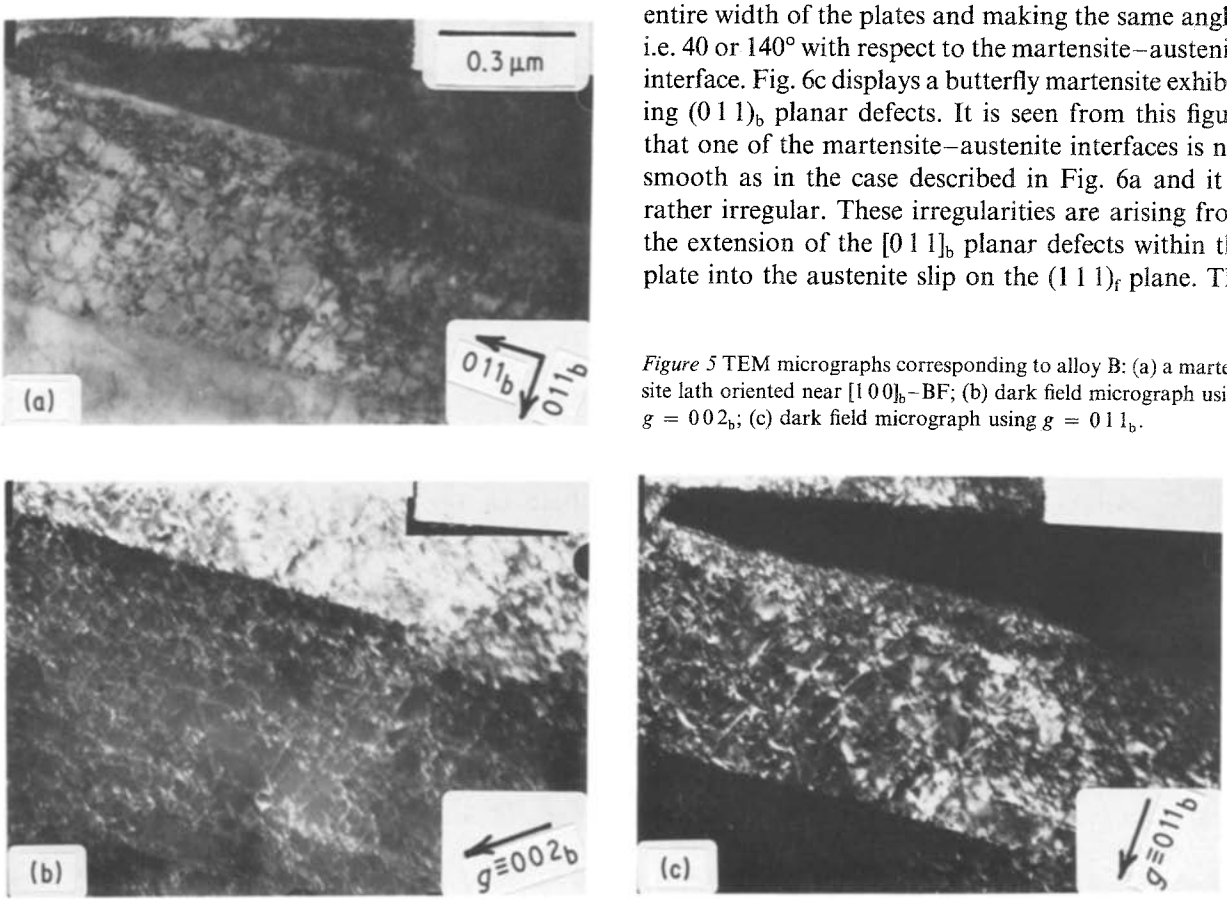

Figure 5 TEM micrographs corresponding to alloy B: (a) a martensite lath oriented near $[1\,0\,0]_b$–BF; (b) dark field micrograph using $g = 0\,0\,2_b$; (c) dark field micrograph using $g = 0\,1\,1_b$.

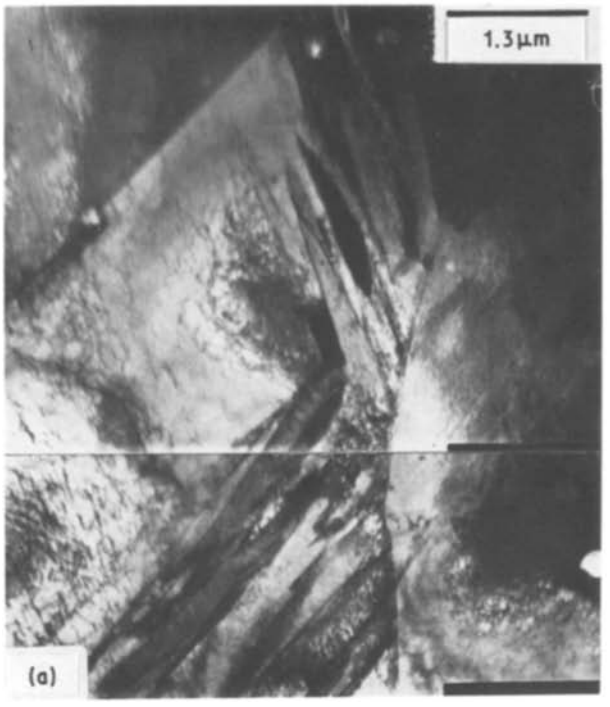

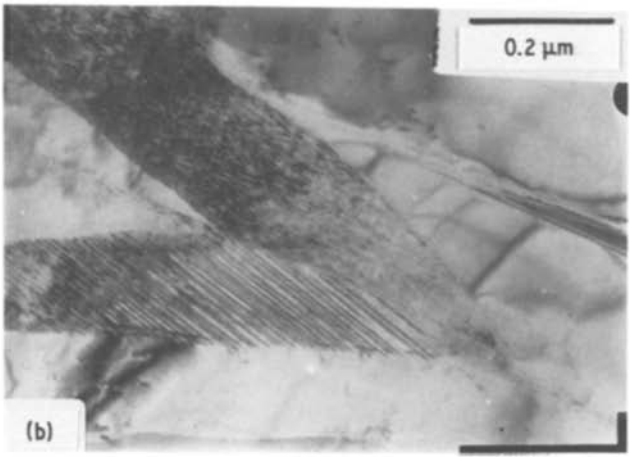

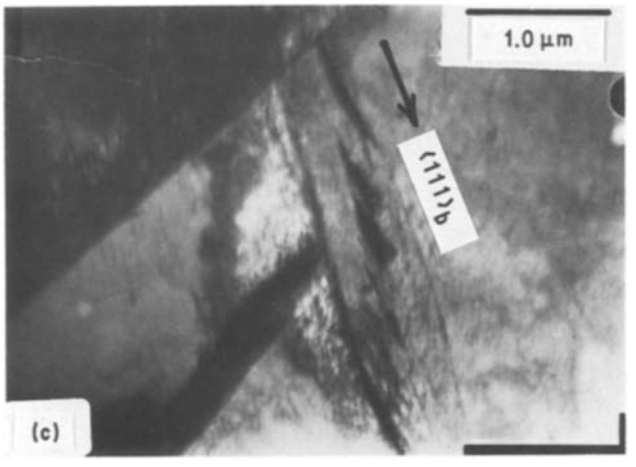

Figure 6 TEM micrographs corresponding to alloy E showing different morphologies of butterfly martensite. For details see text.

dislocation concentration around the martensite–austenite interface is much higher than in the interior of the austenite grain resulting from the accommodation of the shape strain by slip in the austenite. There is no junction plane in Fig. 6b, while the two plates forming the butterfly martensite are touching each other without stopping the growth of the martensite plates on either side. Therefore, in this case, the junction plane should be normal to the plane of the photograph.

In some cases, an array of $[1\,1\,2]_b$ transformation twins around a mid-rib region was observed. The mid-rib was seen to be parallel to the longitudinal direction of the plate. The rest of the plate revealed the presence of $[0\,1\,1]_b$ dislocations on either side of the mid-rib. Several kinks at the martensite–austenite interface, as a result of the association of $(0\,1\,1)_b$ planar defects in the martensite with austenite slip on $(1\,1\,1)_f$, were frequently viewed. Fig. 7 is a diffraction pattern, taken from the martensite–austenite region corresponding to the above mentioned structure. The possible martensite–austenite orientation relationship deduced from this diffraction pattern are,

$$[1\,1\,\bar{2}]_f \sim // [0\,1\,\bar{1}]_b$$

$$(\bar{1}\,1\,1)_f \sim // (0\,1\,1)_b$$

$$(\bar{1}\,1\,0)_f \sim // (\bar{1}\,0\,0)_b$$

as expected from the N–W relationship. The intensity distributions appear to be reasonably symmetrical in this diffraction pattern.

Fig. 8a shows a plate of butterfly martensite composed of two layers separated by a definite boundary. The transformation twins are observed at only the outer surface forming a right angle and appear to extend towards the centre of the plate. Another set of transformation twins are formed at the centre line and appear to extend upwards to the opposite surface of the plate. An electron diffraction pattern taken from the central region of Fig. 8a and covering, at the same

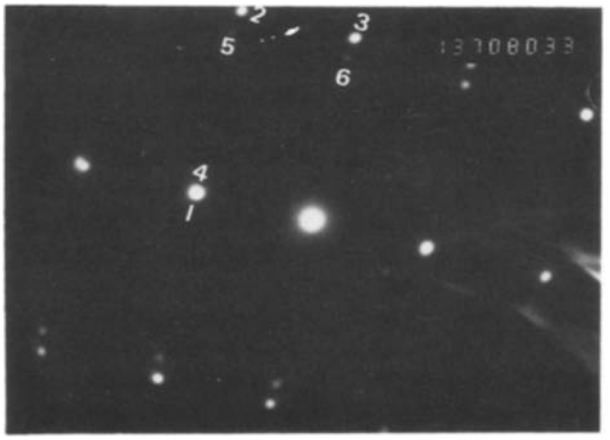

Figure 7 An electron diffraction pattern showing $(1\,1\,1)_f \sim \| (0\,1\,1)_b$ corresponding to butterfly martensite in alloy E.

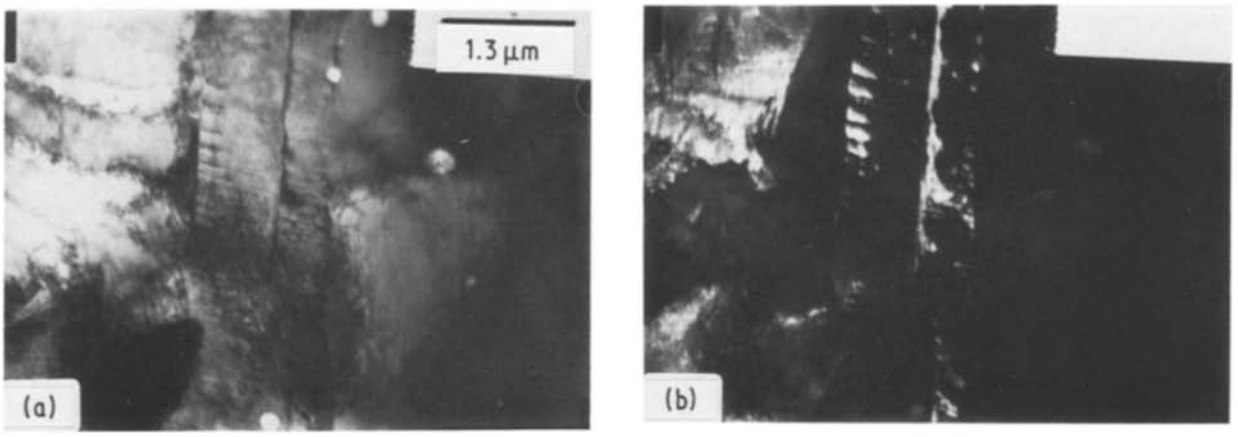

Figure 8 TEM micrographs showing the presence of retained austenite in a butterfly martensite plate in alloy E; (a) BF, (b) DF.

time, both surfaces of the plate were essentially the same as that demonstrated in Fig. 7. A dark field micrograph imaged on a $(\bar{2}\,2\,0)_f$ reflection reveals the retention of austenite on the twin surfaces as well as along the central line, Fig. 8b. This may suggest that the two parts are formed side-by-side, i.e. in a cooperative fashion.

The extent of twins in butterfly martensite was found to vary from one plate to another. Fig. 9 shows arrays of transformation twins parallel to the martensite–austenite interface. Careful tilting brings the twin surface into contrast. Based on this micrograph, the plate thickness is about 0.11 μm and the width is about 0.55 μm. Transformation dislocations can be seen on the twin surface shown in this micrograph. The arrow indicates the presence of a kink in the martensite–austenite interface, probably due to thickening of the plate by motion of the ledges. An electron diffraction pattern positioned on the central portion of the plate revealed that once again we are having the same components of the diffraction described in Fig. 7, leading to the same martensite–austenite orientation relationship, i.e. the N–W relationship.

Tempering at 200° C for 1 h leads to a fast decomposition of the martensite resulting in the formation of ε, η and Fe_3C carbides within the matrix as well as on the twin surfaces, Fig. 10a and b. However, due to the fact that the size of these precipitates is very fine, no measurable change in hardness could be reported.

4. Conclusions

1. Melt spinning of Fe–0.5 wt % C induces a martensitic structure at room temperature even for grains as fine as 3 μm. The martensite is mainly dislocated type with or without fine transformation twins. The martensite laths are separated by thin layers of retained austenite. Both the K–S and the N–W relationships were operating for the martensite–austenite orientations. Some of the martensite laths exhibited a twin relation. The dislocations within the laths were mainly screw type.

2. Retention of austenite ($\sim$ 100%) is enhanced in Fe–Ni–C alloy by the fine grain size ($\sim$ 3 mm) even at liquid nitrogen temperature in the as-melt spun

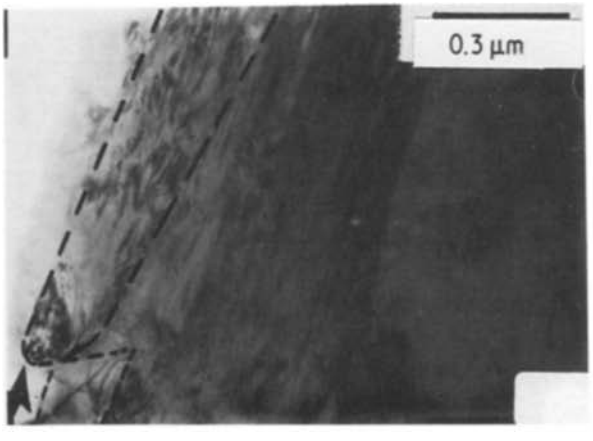

Figure 9 A TEM micrograph showing the presence of retained austenite on the twin surfaces in a butterfly martensite plate in alloy E. Note the thickening of the plate by the motion of lateral ledges.

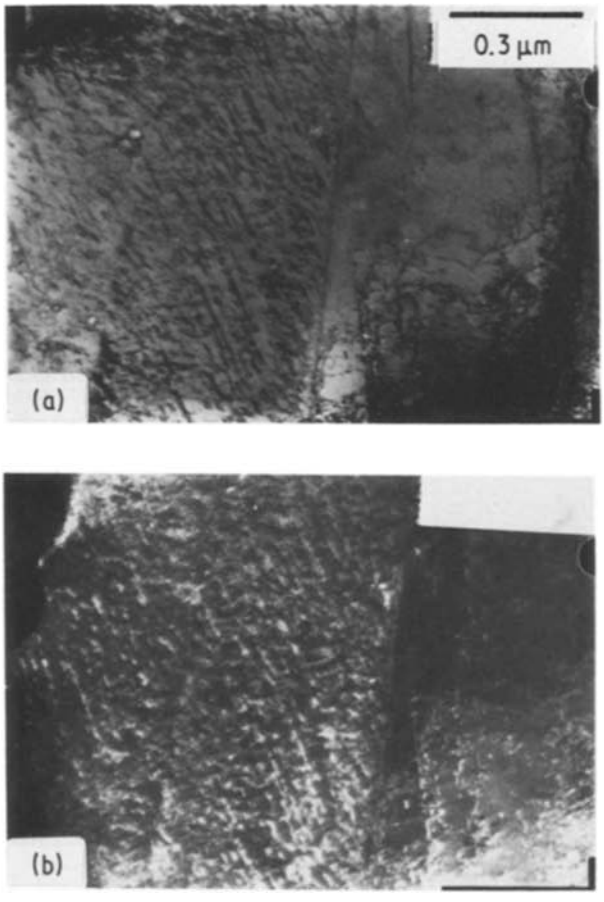

Figure 10 TEM micrographs of a butterfly martensite plate in alloy E tempered at 200° C, showing the presence of fine carbides: (a) BF; (b) DF.

condition. Increasing the grain size by reheating caused martensitic transformation on cooling to $-60°$ C.

3. The present study was concentrated on butterfly martensite: it consists of two wings with no junction plane and forming an angle of 40 or 140°. Each wing is composed of one layer or two layers. The transformation twins within each wing are either parallel to the martensite–austenite interface or normal to it. In some cases the morphology of the martensite wing is similar to a mid-rib plate. The martensite–austenite interface is not always straight and it can be, as well, curved or irregular with many kinks. The martensite–austenite orientation is mainly controlled by the N–W relationship.

References

1. S. K. DAS and G. THOMAS, *Met. Trans.* **1** (1970) 325.
2. G. R. SPEICH, *Trans.-AIME* **245** (1969) 2553.
3. M. SARIKAYA, B. G. STEINBERG and G. THOMAS, *Met. Trans.* **13A** (1982) 2227.
4. G. KRAUSS and A. M. MARDER, *ibid.* **2** (1971) 2343.
5. M. UMEMOTO, E. YOSHITAKE and I. TAMURA, *J. Mater. Sci.* **18** (1983) 2893.
6. Y. INOKUTI and B. CANTOR, *Acta Metall.* **30** (1982) 343.
7. F. H. SAMUEL, *Met. Trans.* **16A** (1986) 127.
8. F. H. SAMUEL, *Practical Metallography* **24** (1987) 58.
9. F. H. SAMUEL, *Z. Metallkde.* **76** (1985) 792.
10. E. R. PETTY, (ed.), "Martensite Fundamentals and Technology" (Longmans, London, 1970).
11. F. H. SAMUEL and D. S. SARMA, *Met. Sci.* **16** (1982) 171.
12. F. H. SAMUEL and A. A. HUSSEIN, *Metallography* **15** (1982) 391.
13. M. UMEMOTO and W. S. OWEN, *Met. Trans.* **5** (1974) 2041.

Received 30 September 1986
and accepted 20 March 1987